Advances in Science and Technology Research Journal, 2026, 20(1), 30–47 https://doi.org/10.12913/22998624/208412 ISSN 2299-8624, License CC-BY 4.0

Evaluation of the influence of the support on the aerodynamic characteristics of the tested object

Zbigniew Czyż¹, Paweł Karpiński^{2*}, Paweł Ruchała³, Jonas Matijošius⁴

- ¹ Faculty of Aviation, Polish Air Force University, Dywizjonu 303 No. 35, 08-521 Dęblin, Poland
- ² Department of Machine Operation and Production Processes Management, Faculty of Production Engineering, University of Life Sciences in Lublin, Głęboka 28, 20-612 Lublin, Poland
- ³ Department of Aerodynamics, Łukasiewicz Research Network Institute of Aviation, Warsaw, Poland
- Vilnius Gediminas Technical University, Laboratory of Experimental Mechanics, Sauletekio al. 11, 10223 Vilnius, Lithuania
- * Corresponding author's e-mail: pawel.karpinski@up.edu.pl

ABSTRACT

In wind tunnel experiments, test models are often mounted using external force balances, which require support structures such as masts. These elements can interfere with the flow field, influencing measured aerodynamic forces and moments. This study investigates the aerodynamic impact of a cylindrical mast used to support a light combat aircraft model in a wind tunnel environment. Numerical simulations were performed in Ansys Fluent to evaluate the aerodynamic interference introduced by the mast. Three methods of determining the aircraft's aerodynamic characteristics were analyzed, with particular attention given to both qualitative and quantitative aspects of mast-induced disturbances. Results show that the mast consistently increases the total drag coefficient across the full range of angles of attack, with the effect most pronounced at lower angles. For example, at $\alpha = -20^{\circ}$, the mast contributes approximately 24% of the total drag. In the near-zero range of $\alpha = -4^{\circ}$ to 4° , where overall drag remains low ($C_D = 0.115-0.148$), the mast's contribution becomes proportionally more significant. This highlights the necessity of accounting for support interference in wind tunnel testing to avoid underestimating drag. In contrast, the mast has a relatively minor effect on lift. Its influence is slightly positive in negative lift regimes and slightly negative under positive lift conditions, but the changes are marginal (about 3% of the maximum lift coefficient) and do not meaningfully alter the overall lift behavior. These findings underline the importance of incorporating mast effects in aerodynamic analysis for accurate interpretation of wind tunnel data.

Keywords: aerodynamics, aerodynamic interference, aerodynamic coefficients, computational fluid dynamics, wind tunnel.

INTRODUCTION

Experimental aerodynamic studies of various objects are conducted using wind tunnels. Wind tunnels facilitate investigations of aircraft models [1–3] or their components, such as empennage, wings, and propulsion system elements [4–6]. They are also extensively utilized in the automotive industry, for example, to reduce vehicle air resistance [7], and in civil engineering to examine wind pressure distribution on building facades [8]. Micro wind tunnels are also used for measuring the aerodynamic forces acting on

small objects, such as cereal seeds [9]. Wind tunnel designs are fundamentally classified based on the air circulation method (open or closed circuit) and the achievable air velocity (subsonic, transonic, and supersonic). There are also special tunnels, such as those simulating icing conditions [10, 11]. Regardless of the tunnel design, the test object must be positioned within the measurement chamber in a secure manner that allows for the operation of measuring instruments. The safety aspect involves mounting the model to remain stationary relative to the airflow during the

Received: 2025.07.02

Accepted: 2025.09.19

Published: 2025.11.21

measurement procedure. The balance and sting are subjected to variable loads resulting from the airflow interaction. Therefore, it is essential to ensure high sting stiffness, which enables the secure mounting of the model within the wind tunnel [12]. Simultaneously, the mounting of the object should allow for the operation of a force balance, which measures the aerodynamic forces and moments acting on the model during testing. Consequently, several typical methods for mounting the object within the measurement chamber are employed. Mounting involves the use of supports attached to the walls of the wind tunnel's measurement chamber, with the test object installed at their mounting points. These include wire support, strut support, and sting support. Regardless of the model mounting method within the measurement chamber, the support must ensure the maintenance of the model's aerodynamic center position with changes in the model's angular position relative to the airflow direction [13]. In the case of strut support, the test model is installed on a support mast, while the measurement system is located outside the measurement chamber. The most commonly employed mounting method in low-speed wind tunnels is rear-mounted support. In such cases, the most significant distortion of the aircraft model's aerodynamics occurs in its aft region, specifically in the area of the empennage and tail. The rear-mounted mast typically takes the form of a cylinder, often stepped with smooth transitions between successive diameters. Support interference can lead to incorrect measurements of aerodynamic forces, moments, and drag characteristics. This can result in inaccurate predictions regarding the behavior of the real-world object in flight. Therefore, it is crucial to evaluate this phenomenon and attempt to minimize its impact on the overall aerodynamic characteristics of the test object. Minimization of interference effects can be achieved through modifications to the support's shape to reduce aerodynamic drag. Numerical simulations aimed at designing a fairing around the support to mitigate its aerodynamic interactions with the fuselage boundary layer are presented in reference [14]. Another method involves the correction of data obtained from both numerical and empirical techniques. The mast constitutes an additional source of aerodynamic drag. Its presence disrupts the velocity and pressure fields around the test model (e.g., aircraft). This disruption results in the phenomenon of aerodynamic interference,

which occurs when two or more objects are within an airflow and interact aerodynamically. The airflow around one object influences the airflow around the other, potentially leading to changes in the aerodynamic forces acting on these objects. Support disturbances are a significantly greater concern in dynamic testing than in static testing [15]. This issue is further complicated by the fact that mutual aerodynamic interactions vary with the test model's angle of attack. Tilting the object results in a change in the mast's orientation relative to the incoming airflow, which, considering the mast's geometry, causes a change in the aerodynamic forces generated on it. A compilation of literature dedicated to the topic of support interference of wind tunnel models is presented in reference [16]. The issue of sting support interference was analyzed by Carter [17]. It was shown that a rear support housing carrying a sting and a vertical incidence strut will induce a pressure gradient on the model, which will lead to an increase in axial buoyancy force. Studies on a diamondshaped support were conducted in reference [18]. The advantage of this solution is a reduced impact on lift due to its conical profile. The analysis of this mutual interaction between the model and the mast can be conducted using various techniques. The first is direct wind tunnel measurements using a force balance [19]. Complementary to this method is the velocity field imaging method, such as PIV (particle image velocimetry) or Schlieren imaging. The second method involves the use of numerical simulations based on computational fluid dynamics (e.g., CFD) [20]. This technique involves creating a digital model of the test object and defining physical models related to airflow. This method can be used to model the velocity and pressure fields around an aircraft [21] and other aerodynamic objects [22, 23]. Both of these approaches were applied in studies of dummy strut interference with a large transport aircraft model [24]. In this study, attention was paid to the importance of corrections related to the Mach number and angle of attack in transonic flows, for both wind tunnel tests and calculations.

Beyond these applications, CFD has also been employed in a wide range of other aerodynamic studies. Examples include the analysis of turbulence evolution in a fan rig under boundary layer ingestion (BLI) conditions using the URANS (Unsteady Reynolds-Averaged Navier-Stokes) approach [25], as well as the evaluation of a vertical axis wind turbine with adjustable blade pitch,

enabling torque and power analysis across different speeds [26].

The selection of parameters related to model support in the wind tunnel and selected aspects related to their optimization are presented in reference [27]. Numerical calculations were performed using the CFD method. This method can also be used to calibrate the flow in the wind tunnel measurement chamber and to assess support and wall interference according to commonly accepted experimental procedures [28]. CFD simulations encompassing wind tunnel interference effects can be used to validate the numerical model [29]. A comparison between the results obtained in the wind tunnel and simulations revealed the extent of modeling error introduced by neglecting the support structure [30]. Although study [31] primarily focuses on wind tunnel experiments, it also incorporates a comparison with 2-D CFD simulations of a NACA 0018 airfoil, revealing discrepancies between numerical and experimental predictions of lift and drag.

The results of an experimental study on the influence of model support on the determination of aerodynamic coefficients in a wind tunnel are presented in reference [32]. It was found that the main disturbances pertain to the yawing moment coefficient. The results of aerodynamic coefficient calculations without disturbances for a training aircraft model were compared with experimental data. Studies on the aerodynamic interference of support with a road vehicle model are presented in references [33, 34]. The conducted tests revealed a slight increase in drag and a larger increase in lift due to interference with the upper support. It was observed that wheel supports increase lift. The effects of support interference were analyzed in [35, 36], where CFD results with and without the support structure were compared. The studies demonstrated that the influence of support interference on the model can be appropriately corrected using Mach number correction and buoyancy correction methods for forebody drag. Strut interference for various angles of attack and sideslip in the case of a turboprop transport aircraft model was analyzed by Russo [37]. The issue of strut interference in high-speed flows is more complex due to the physics of the phenomenon, which can lead to the presence of shock waves or flow separation in regions of high-pressure gradients. Interference for high Mach numbers and cylinder and rhombus models was investigated by Lee [38]. Aerodynamic interference of a strut

with external and internal pivots was studied in reference [39]. Hebbar and Sommers [40] investigated the aerodynamic interference of a strut designed for mounting a lightweight fighter prototype. The analysis revealed that interference reduction can be achieved by attaching the forward struts to the wing tips and the aft strut to the tail hook pivot point. Another analysis of tests for two combat aircraft configurations revealed the existence of unsteady interference phenomena in the wind tunnel involving coupling between support and wall interference mechanisms [41].

It should be noted that the mast is not the only source of aerodynamic interference present in wind tunnel conditions. The interaction of the tunnel walls and floor can also be significant – the floor can induce an effect similar to ground effect, altering the angle of deflection of the wake behind the wing of the investigated object. Eventually, the wake may change its position versus the tail [42]. On the other hand, this effect is easily mitigated by increasing the distance from the floor.

In this paper, the aerodynamics of an aircraft in the form of a trainer/combat aircraft mounted on a strut support (Figure 1) with external force and moment measurements, which was the subject of consideration in reference [43], are analyzed.

The mounting took the form of a single strut in the shape of a stepped cylinder. Particular attention was paid to the aerodynamic interference of the aircraft model and the mast. The studies were conducted using the CFD method. For this purpose, a geometric model of the test object was developed and placed in a created computational domain. Then, a computational mesh was generated, and the parameters of the flow model were defined. A series of calculations were performed for various angles of attack. Subsequently, a quantitative and qualitative analysis of the mast's influence on the aerodynamics of the aircraft model itself was performed.

RESEARCH OBJECT AND METHODOLOGY

The Alenia Aermacchi M-346 Master aircraft was selected as the reference object for the development of the aircraft model in this study. This selection was based on its operational use at the Polish Air Force University. The M-346 Master (designated "BIELIK" in the Polish military) is a tandem-seat, twin-engine aircraft designed for advanced flight training. In the initial phase, a 1:48



Figure 1. (a) Wind tunnel used for experimental studies and (b) a view of the test object (an Alenia Aermacchi M-346 Master model) during wind tunnel testing [43]

scale physical model was used to generate the digital aircraft model. A 3D scanning technique was employed using a Nikon scanner equipped with a non-contact Model Maker MMDx scanning head. Geomagic Design X software was utilized to capture and map the geometry of the target object. The scanning process resulted in a point cloud dataset, which was processed within the software to create a detailed 3D mesh. Subsequently, SolidWorks software was used to construct the final aircraft model based on the processed geometry from Geomagic Design X.

The prepared model was used to conduct a numerical aerodynamic analysis, incorporating minor simplifications to facilitate the proper generation of the computational mesh necessary for numerical calculations. In the Ansys Meshing module, computational meshes were generated by selecting appropriate element sizes corresponding to the characteristic dimensions of the computational domain. Due to the specifics of the calculations, three independent computational domains were prepared. In order to evaluate the influence of the mast on the aerodynamic characteristics of the aircraft under study, the following variants were prepared:

- 1. Flow around the aircraft alone, positioned within the measurement space.
- 2. Flow around the aircraft with the mounting mast
- 3. Flow around the mast alone, without the aircraft.

The results for variant I, obtained through numerical simulation, can serve as reference values, as they pertain to the aircraft alone. For the sake of order, this variant is designated as the first (1) method for determining the aircraft's characteristics. The second (2) method for determining the aerodynamic characteristics of the aircraft can be based on variants II and III. In this method, the aircraft's characteristics are determined by subtracting the forces and moments obtained in variant III (for the mast alone) from the values of forces and moments acting jointly on the mast and aircraft from variant II. A third (3) method for calculating the values of forces and moments acting on the aircraft alone can also be considered, by appropriately partitioning the domain and reading these values separately in variant II (CFD method provides this capability). All of the mentioned methods are presented graphically in Figure 2.

For the aforementioned variants, computational meshes were generated using the tetrahedral method with the patch conforming algorithm. A prism layer consisting of 5 layers with the Smooth Transition Option was defined on the wall surfaces. For variant I, the skewness index was 0.93844, for variant II it was 0.82435, and for variant III -0.94025. The generated mesh in variant I consisted of 6,908,751 elements with 1,915,778 nodes, in variant II it consisted of 955,343 elements with 248,836 nodes, and in variant III, 6,088,803 elements with 1,690,000 nodes, respectively. The thickness of the prism layer was determined based on the flow type defined by the Reynolds number. The mesh plays a very important role in CFD simulations, as the type and quality of the mesh determine the accuracy of the calculations. A view of an example mesh is shown in Figure 3.

Figure 4 illustrates the considered computational domains encompassing the aforementioned

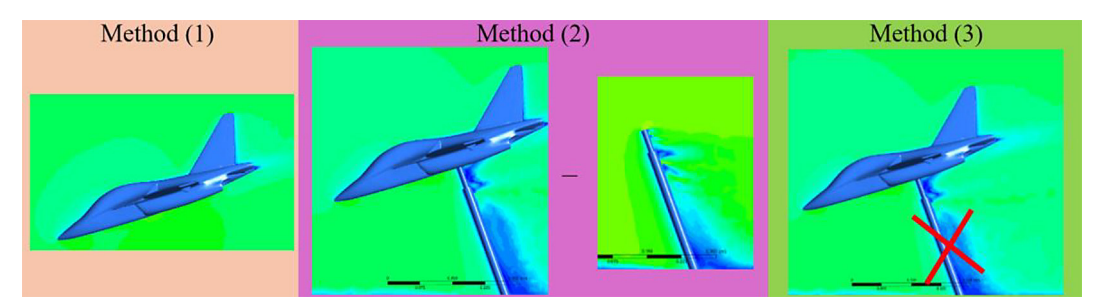


Figure 2. Graphical representation of three approaches (methods) aimed at determining the aerodynamic characteristics of an aircraft: method (1) – flow around the isolated aircraft, method (2) – flow around the aircraft with the mast, reduced by the flow around the mast alone, method (3) – flow around the aircraft with the mast, but without accounting for the mast itself

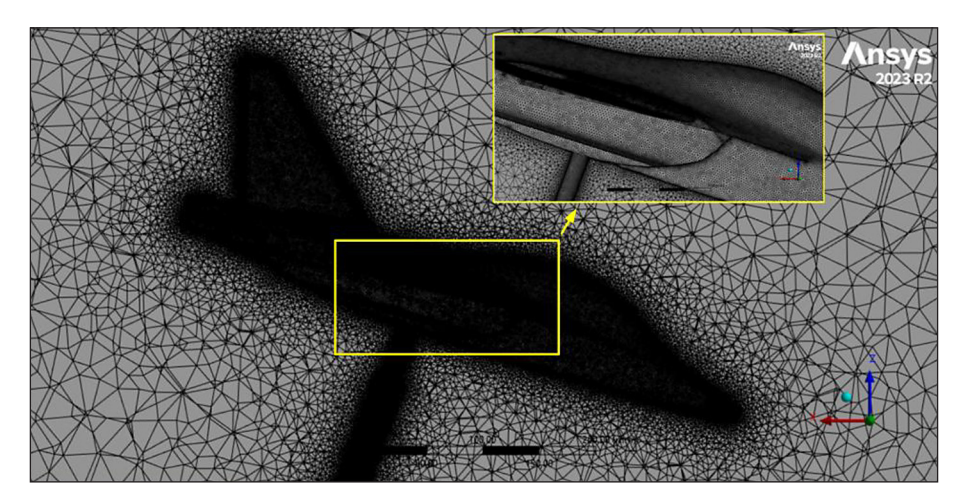


Figure 3. View of an example mesh for variant I, encompassing the aircraft model and mast

three research object variants. Each variant was enclosed within a domain measuring $700 \times 700 \times 1500$ mm (width × height × length). These dimensions are adequate for the measurement space dimensions of the wind tunnel in which the experiment was conducted.

The calculations were performed for a threedimensional, turbulent, steady-state flow. Ansys Fluent software, which is based on the finite volume method, was used for this purpose. The coupled method was applied to solve the pressurevelocity coupling equations. Second Order Upwind discretization schemes were selected for the spatial discretization of turbulent kinetic energy, turbulent dissipation rate, energy equation, and pressure. The k- ω SST (shear stress transport) turbulence model was selected for the numerical analysis. This model introduces two additional transport equations into the Reynolds-averaged Navier-Stokes equations: one for the turbulent kinetic energy and one for the turbulent dissipation rate. The k- ω SST turbulence model was chosen due to its relatively accurate representation of turbulence in the near-wall region, as well as its low sensitivity to inlet turbulence boundary conditions. In the next step, the boundary conditions were defined. The CFD geometric model has one inlet and one outlet. The air inlet to the computational domain was set as a velocity-inlet with a value of 40 m/s. The outlet from the domain was set as a pressure-outlet, and the outlet pressure was set to standard atmospheric pressure. Physical parameters such as air density and viscosity were set for a temperature of 299 K and were 1.177 kg/m³ and 1.85·10-5 kg/(m·s), respectively.

RESULTS

Analysis of variant I

Frist variant involves calculations of the aircraft model alone, without the mast. The results obtained in this manner will serve as a reference value. They are presented in the form of basic characteristics in Figure 5. For the considered

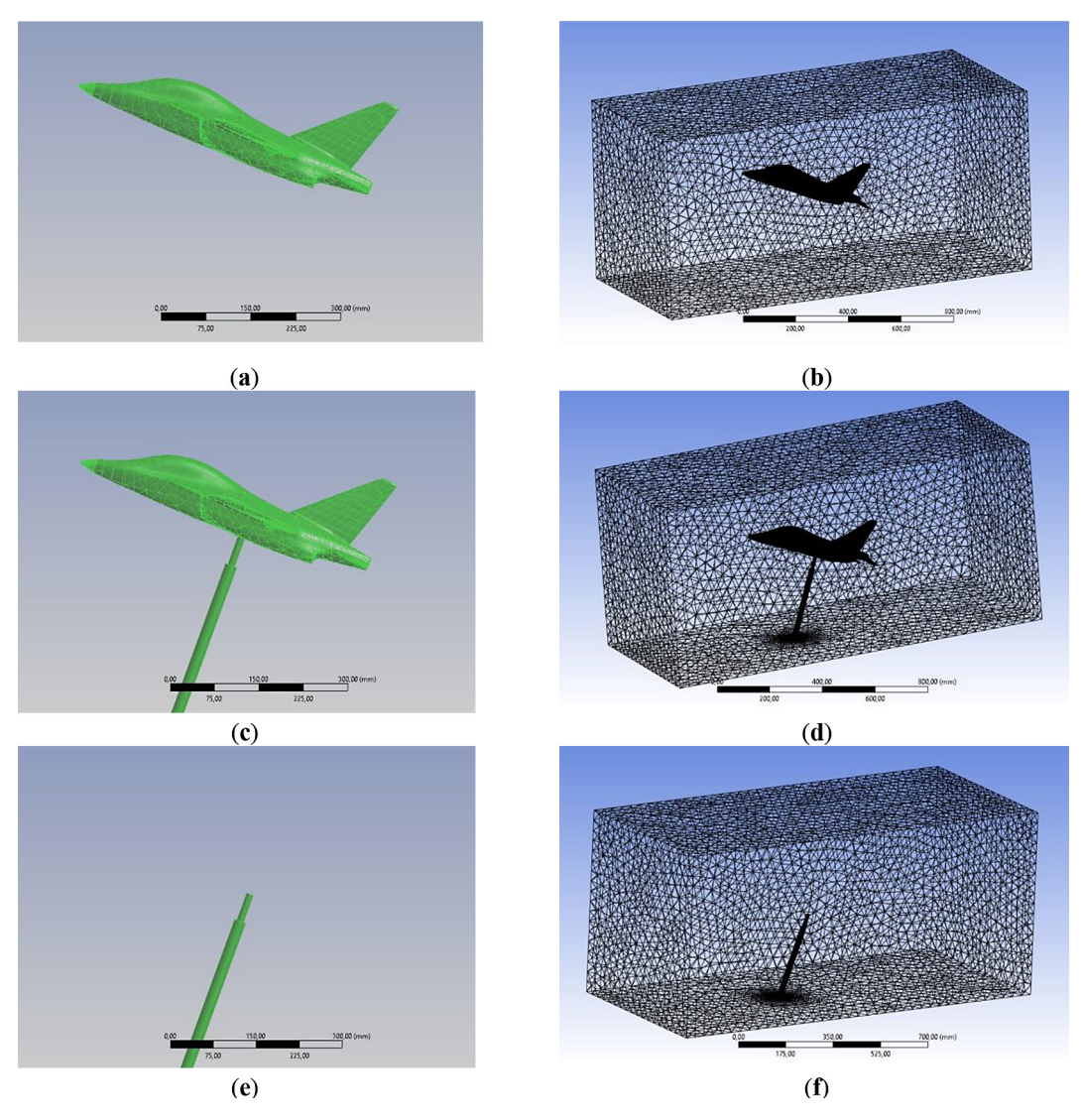


Figure 4. View of the considered research objects (left) and the computational domains created for them (right) for: (a), (b) variant I; (c), (d) variant II; (e), (f) variant III

case, in the range of negative angles of attack, the drag coefficient increases with the pitching of the aircraft model, where at $\alpha = -20^{\circ}$, the C_{x} value is 0.238. The minimum value of 0.038 is reached at $\alpha = -4^{\circ}$. The drag coefficient C_{r} value for an angle of attack $\alpha = 0^{\circ}$ is 0.047. In the range of positive angles of attack, the drag coefficient increases with the increase of the angle of attack. Initially, the increase is slow – from a value of C_{x} = 0.047 for $\alpha = 0^{\circ}$ to $C_{r} = 0.075$ for $\alpha = 4^{\circ}$. Then, this increase becomes faster, reaching a value of $C_r = 0.500$ for $\alpha = 20^{\circ}$. The increase in drag in this range may be caused by the increasing frontal area and the intensification of flow separation phenomena, which causes greater disturbances and aerodynamic drag.

The relationship between the lift coefficient C_z and the angle of attack α largely indicates

a typical, linear increase in lift with increasing angle of attack (in the range from -16° to 8°), reaching a maximum value at $\alpha = 20^{\circ}$. At an angle of attack of 0°, the aircraft model generates positive lift, which is justified by its asymmetry. In the range of negative angles, the lift coefficient C_{\perp} is negative. At $\alpha = -20^{\circ}$, the C_z value is -0.846, indicating a significant downward force. With smaller negative angles of attack (approaching 0°), the lift coefficient increases until it reaches a value close to zero at $\alpha = -4^{\circ}$. For $\alpha = 0^{\circ}$, the C_{\perp} value is 0.328. For positive angles of attack, the lift coefficient increases almost linearly with the increase in the angle of attack. Starting from C = 0.328 at α = 0°, the C_z value increases to 1.043 at $\alpha = 20^{\circ}$. This increase is relatively rapid up to 8° and indicates effective lift generation with an

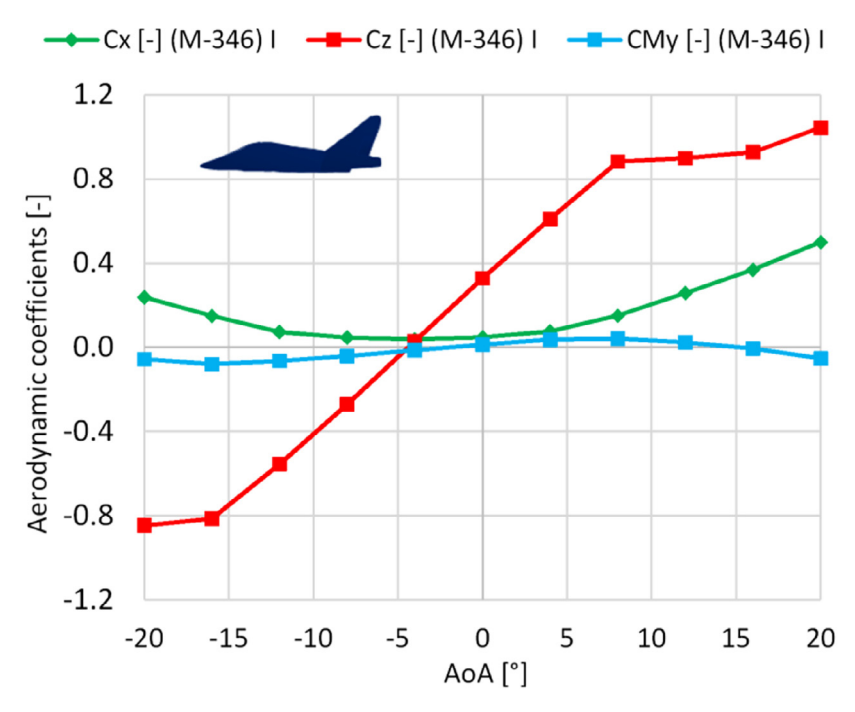


Figure 5. Relationship of aerodynamic coefficients to the angle of attack for the considered variant I

increase in the angle of attack. At larger angles, the lift coefficient still increases, but more slowly.

The C_{My} values are initially negative, indicating that the aircraft has a tendency to pitch down (nose-down). The smallest C_{MV} value of -0.080was observed at $\alpha = -16^{\circ}$. As the angle of attack increases, the C_{My} values increase (with smaller absolute values), suggesting a decrease in the pitching tendency. For further increases in the angle of attack, C_{Mv} assumes positive values, reaching a maximum value of $C_{My} = 0.041$ at $\alpha = 8^{\circ}$. However, at even larger angles of attack, the C_{Mv} coefficient begins to decrease again, reaching a negative value of $C_{My} = -0.053$ at $\alpha = 20^{\circ}$. The prepared model, representing the actual aircraft, does not exhibit stability within the required range, but this may be due to inaccuracies in its representation. However, this issue is not the subject of this work, and in the following section, the influence of the mast mounting the aircraft model in the tunnel will be discussed.

Analysis of variant II

The approach presented above enables the analysis of aerodynamic forces and moments acting on the object under study. The selected CFD-based method allows for the reading of forces or moments on any (previously defined) surface of the object. In the considered case for variant II,

which reflects the conditions in the tunnel, i.e., includes both the aircraft model and the mast, it was decided to separately present the loads on these elements. As shown in Figure 6, the characteristics of the mast will be indicated in red, the aircraft in green, and the mast and aircraft combined in blue. It should be noted that at this stage, the results for these two elements are considered, but within the same shared flow (as in a wind tunnel). Consequently, the results reflect their aerodynamic interference.

Figures 7 and 8 show the characteristics of the drag coefficient, lift coefficient, and pitching moment coefficient for variant II, respectively. The green data series pertains only to the aircraft model, while the red series pertains to the mast. The blue data series represents the sum of these two previous series. In reality, an external aerodynamic balance measures the forces in a summed manner, and there is no direct method to identify the forces separately on the considered surfaces. Analyzing the results for variant II, which present the aerodynamic coefficients for the M-346 aircraft model and the mounting mast as a function of the angle of attack α , we can draw the conclusions presented below.

For negative values of the angle of attack, the drag coefficient C_x gradually decreases, reaching the lowest value around $\alpha = -4^\circ$. Then, with an increase in the angle of attack, C_x starts to increase

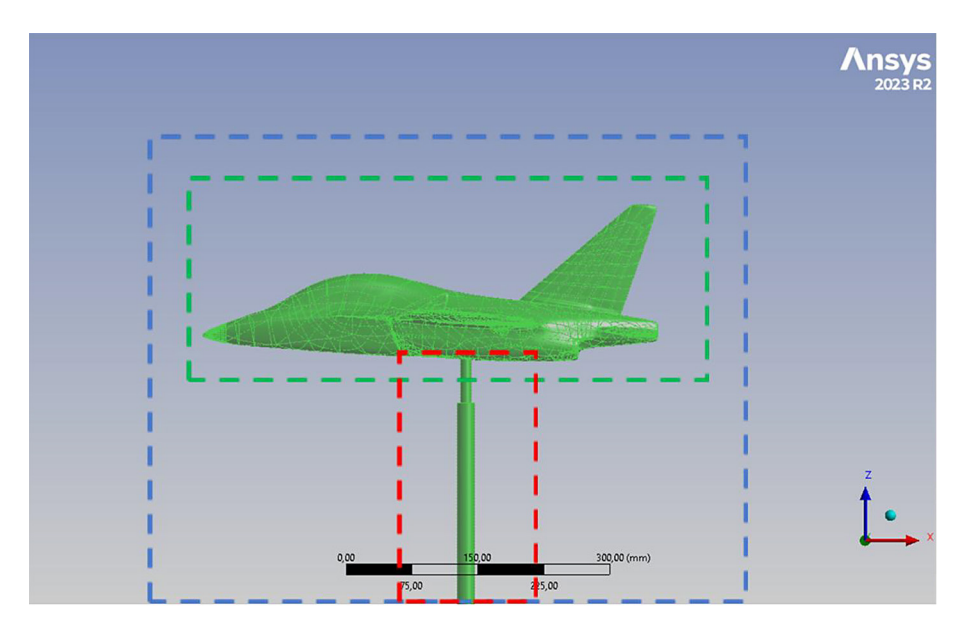


Figure 6. Graphical representation of the model with identification of separated elements for analysis

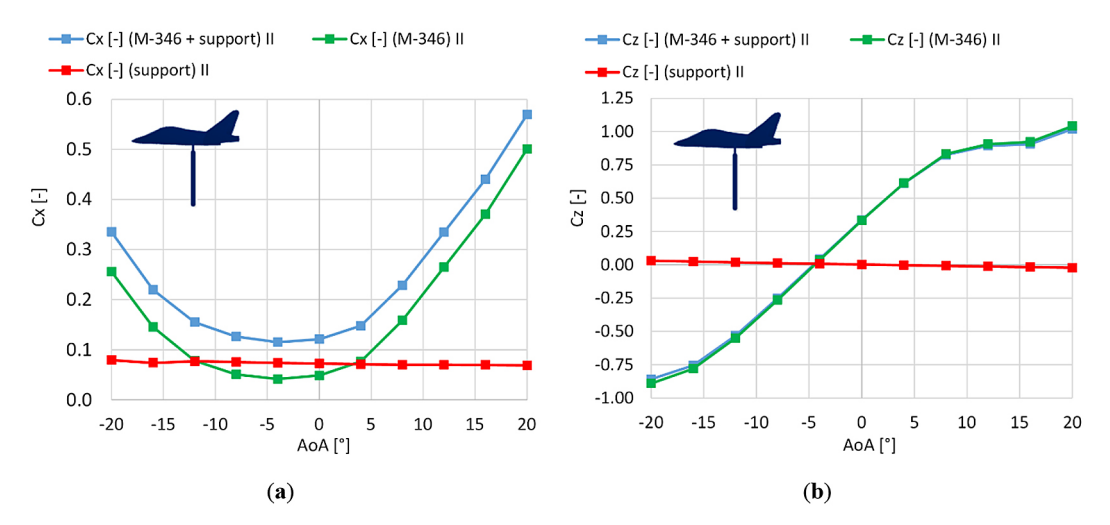


Figure 7. (a) Relationship of aerodynamic drag coefficient C_x to angle of attack and (b) relationship of lift coefficient C_z to angle of attack for the studied object, with separation of aircraft and mast

again, reaching maximum values for positive values of the angle of attack. The lowest value of the aerodynamic drag coefficient, approximately $C_x = 0.042$, was obtained at an angle of attack $\alpha = -4^{\circ}$. This is the point at which the aerodynamic drag force acting on the aircraft is the smallest.

At positive angles of attack, the value of the aerodynamic drag coefficient increases significantly, which is consistent with expectations. For larger angles of attack (above $\alpha=8^{\circ}$), the increase in C_x becomes more rapid, suggesting increased air flow disturbances around the wing and other non-linear aerodynamic effects. The $C_x(\alpha)$ curve is not symmetrical with respect to the axis $(\alpha=0^{\circ})$. The C_x values for large negative angles of attack

are smaller than for the same positive values. This means that drag increases more rapidly for positive angles of attack. In the case of the aerodynamic drag coefficient C_x for the mast, relatively small changes were observed throughout the entire range of angles of attack α . The C_x values oscillate around an average value of approximately 0.073, indicating relatively stable aerodynamic properties of the mast, regardless of the angle of attack. In contrast to the results for the aircraft model, the mast's drag coefficient does not show a significant increase or decrease as a function of the angle of attack. For an angle $\alpha = 20^\circ$, the C_x coefficient is 0.069 while for $\alpha = -20^\circ$, it takes a value of 0.080. These differences are small and do

not significantly affect the overall aerodynamic drag generated by the mast.

The summed aerodynamic drag force characteristic for the aircraft and mast shows a similar trend to the drag force characteristic for the aircraft alone. This is due to the practically constant drag force value of the mast, which only caused an upward shift of the aircraft's characteristic. The C_{x} values for the "aircraft + mast" assembly increase from 0.115 at $\alpha = -4^{\circ}$ to 0.569 at $\alpha = 20^{\circ}$. Based on this, it can be concluded that the mast contributes to an increase in the C_{ν} values throughout the angle of attack range, but its influence is more noticeable at smaller angles of attack. For negative angles of attack, the mast adds a significant portion to the total drag, as seen in the example of $\alpha = -20^{\circ}$, where the mast's drag constitutes approximately 24% of the total drag. In the angle of attack range from $\alpha = -4^{\circ}$ to $\alpha = 4^{\circ}$, the total aerodynamic drag coefficient is relatively low, reaching values from 0.115 to 0.148. In this zone, the drag generated by the mast constitutes a significant portion of the total drag, suggesting that in real tunnel experiments, the mast's influence should be considered for accurate representation of the aircraft's aerodynamic characteristics. At angles of attack greater than $\alpha = 8^{\circ}$, the total drag coefficient begins to increase rapidly, reaching a value of 0.569 at $\alpha = 20^{\circ}$. In this zone, the mast's drag becomes less significant compared to the drag generated by the aircraft, which may result from the intensification of vortex phenomena on the aircraft's wing.

The sum of the lift coefficients for the aircraft and mast exhibits a typical trend for this type of object, where with an increase in the angle of attack α , the value of the lift coefficient C_z increases. The largest value of the C_z coefficient, equal to 1.020, was achieved at an angle of attack $\alpha = 20^{\circ}$. The mast introduces some disturbances in the lift force values, but its influence is small compared to the values obtained by the aircraft. At an angle of attack $\alpha = 0^{\circ}$, the lift force increases from 0.334 to 0.337, indicating a marginal effect of the mast on the total lift force in this configuration. For positive angles of attack, the mast slightly lowers the C_z values, e.g., at $\alpha = 20^\circ$, the total C_z coefficient is 1.020, while for the aircraft alone it would be 1.042. This value is lowered by the negative contribution of the mast, which may result from its interference with the airflow under the fuselage and wings of the aircraft. For negative angles of attack, the mast has a positive contribution to the

total lift force, e.g., at $\alpha = -20^{\circ}$, the C_z coefficient increases from -0.890 to -0.859, indicating some improvement in lift, although these values still remain negative, which is characteristic of aerodynamic configurations at negative angles of attack. Overall, the mast does not introduce significant disturbances to the course of the lift force characteristic. In conditions of generating negative lift, its influence is positive, while at positive lift, this influence is negative, but in both cases the changes are relatively small (on the order of 3% of the maximum value) and do not significantly affect the overall lift force characteristic.

Analysis of variant III

Variant III, as depicted in Figure 2, involves the flow around the mast alone. The analysis of basic aerodynamic coefficients was conducted for the same range of angles of attack. In this case, there is no interaction between the mast and the aircraft model. The C_x values are relatively close to each other, ranging from 0.070 to 0.074 (Figure 9). However, it can be observed that C_x initially increases in the range of angles of attack from -20° to -8° , then begins to decrease down to a value of 20°. The maximum C_x value (0.074) occurs at an angle of attack of -8° , while the minimum (0.070) occurs at an angle of 20°. It is worth noting that the distribution of the C_x coefficient as a function of the angle of attack is not symmetrical with respect to the 0° angle. The C_{x} values are higher for negative angles compared to their counterparts on the positive side. For example, at an angle of attack of -20° , the C_{x} coefficient is 0.073, while at 20° it is 0.070. This difference may result from the fact that when tilted forward, air tends to flow along the leading edge towards the floor of the tunnel measuring space, and when tilted backward – towards the free end of the single strut support. Nevertheless, compared to the higher value, this difference is only 5%.

The C_z coefficient values show a clear dependence on the angle of attack α . For angles of attack from -20° to 20° , a gradual decrease in C_z values is observed. At negative angles (from -20° to 0°), the C_z coefficient is positive. However, its value decreases with decreasing angle of attack, reaching a value close to zero at an angle of 4° . It should be noted that the behavior of the C_z coefficient is not symmetrical with respect to the angle of attack $\alpha = 0^{\circ}$. The values for negative angles are larger (positive) compared to their counterparts on

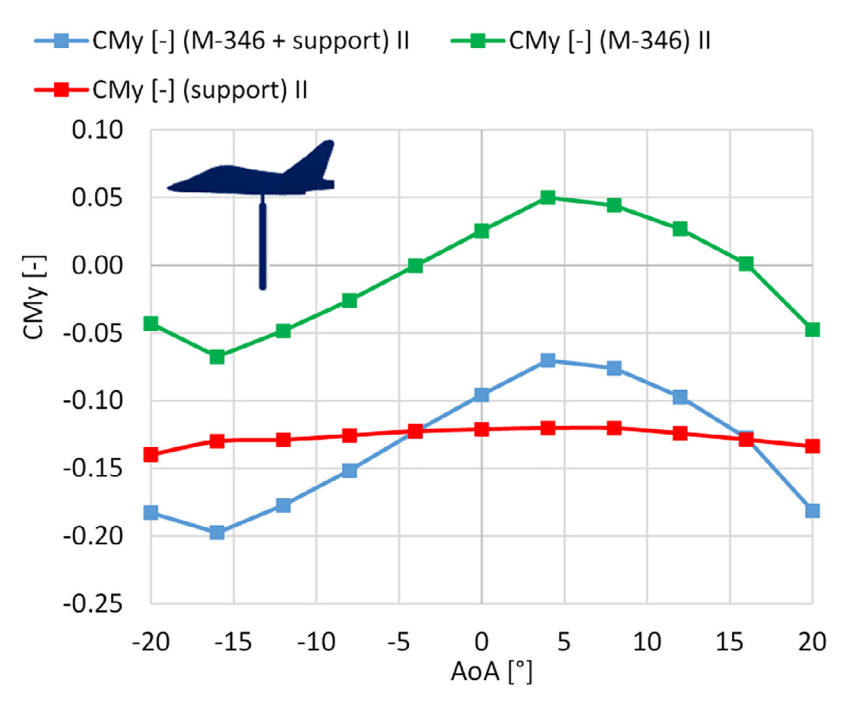


Figure 8. Relationship of pitching moment coefficient C_{My} to angle of attack for the studied object, with separation of aircraft and mast

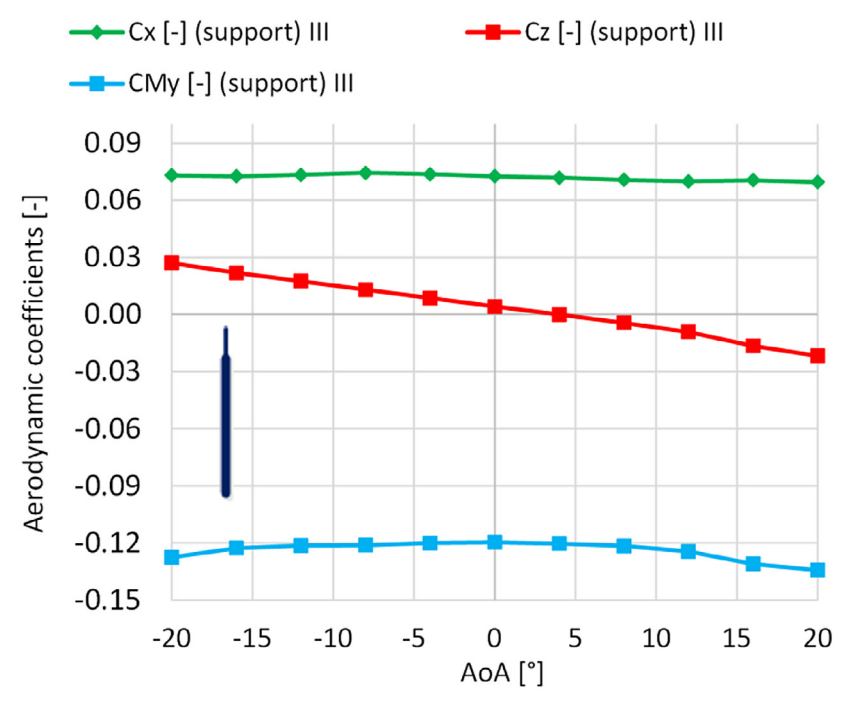


Figure 9. Relationship of aerodynamic coefficients to angle of attack for the considered variant III

the positive side. At angles of -20° and 20° , the C_z coefficient reaches its extreme values: for -20° it is 0.027, and for 20° it is -0.022. The largest positive value of the C_z coefficient (0.027) occurs at an angle of attack of -20° , which means that in this range the lift force is the largest. For positive angles, the lift force begins to act downwards,

and the largest negative value of the C_z coefficient (-0.022) occurs at an angle of attack of 20°. The results suggest that the influence of the lift force generated by the mast on the lift force of the entire system (aircraft+mast) is negligible.

In the case of the $C_{\it My}$ characteristic, it should be noted that the values are negative for the entire

range of angles of attack. This indicates the action of the pitching moment in one constant direction and is natural: the moment is expressed relative to the aircraft's center of gravity, which is consistently located above the mast. Thus, the mast's drag force always results in a negative moment (tendency to pitch down). The C_{Mv} coefficient values generally decrease (become more negative) with an increase or decrease in the angle relative to the value at an angle of attack of 0°. In the range of angles from -12° to 4° , the C_{Mv} coefficient values are relatively stable, with small fluctuations around -0.120. The smallest pitching moment value (least negative) occurs at an angle of attack of 0° and is -0.120, indicating a minimal pitching moment at this point. At higher angles of attack (above 12°), the C_{Mv} coefficient values rapidly decrease (become more negative), reaching the lowest value (-0.134) at an angle of attack of 20°. The distribution of the C_{Mv} coefficient values is not symmetrical with respect to the 0° angle. For negative angles (from -20° to 0°), the C_{Mv} values are slightly smaller (less negative) than for their corresponding positive angles. For example, at an angle of -20° , the C_{My} coefficient value is -0.128, while at 20° it is -0.134. These conclusions highlight the significance of the angle of attack in shaping the pitching moment acting on the mast, which can be crucial for interpreting wind tunnel results for the tested model.

Analysis of the velocity and pressure fields around the studied object

The results in the form of velocity and pressure contours are presented in Figures 10, 11, and 12, respectively, for selected angles of attack, i.e., -20°, 0°, and 20°. Analyzing the velocity field results, several significant dependencies can be observed, describing the influence of the mounting mast on the velocity. In the considered case for variant II, for all angles of attack (-20° , 0° , 20°), the maximum velocity is higher compared to the reference variant I. The largest difference occurs at an angle $\alpha = -20^{\circ}$ and is +1.855 m/s, and the smallest at an angle $\alpha = 0^{\circ}$, i.e., +1.105 m/s. This indicates that the presence of the mast affects the acceleration of the flow around the model, which may result from additional aerodynamic interference or a local increase in the stream velocity. In the case of variant III, the maximum velocity is significantly lower compared to the reference variant I for all angles of attack. For an angle

 α = -20°, the difference is as much as 16.54 m/s, for α = 0°, i.e., -2.765 m/s, and for α = 20°, i.e., -12.86 m/s. This means that the mast itself does not cause a significant acceleration of the flow. Based on the above, it can be concluded that the mounting mast influences the increase in the maximum velocity around the aircraft, which may change its aerodynamic characteristics. The mast itself generates significantly lower maximum velocities compared to the aircraft alone. At larger inclinations relative to the angle α = 0°, the velocity differences are more pronounced, which may indicate significant aerodynamic effects related to the interference of the mast and the model.

Analyzing the maximum pressure values on the aircraft model surface for different variants and angles of attack, it can be seen that for all angles of attack, the pressure values in variant II are higher than in variant I. The largest difference occurs at an angle $\alpha = 0^{\circ}$, and the smallest at an angle $\alpha = 20^{\circ}$. They are +54.4 Pa and +1.15 Pa, respectively. This indicates that the presence of the mast increases local pressure values. In the case of variant III, for angles $\alpha = -20^{\circ}$ and $\alpha = 0^{\circ}$, the pressure is higher than in variant I, which may indicate the presence of a high-pressure region on the mast surface itself. However, for an angle $\alpha = 20^{\circ}$, the pressure is significantly lower, suggesting that in this configuration, the flow around the mast generates lower maximum pressure values. For large angles of attack, the mast influences the deflection of air streams in such a way that it does not cause such large pressure increases as the aircraft model itself. For α = 0°, the difference between variant I and variant II is as high as 54.4 Pa, which may mean that at an angle of 0°, the presence of the mast most strongly affects the pressure distribution. For angles $\alpha = -20^{\circ}$ and $\alpha = 20^{\circ}$, the differences are smaller, suggesting that the influence of the mast on the maximum pressure values decreases at larger angles of attack.

Taking this into account, it can be concluded that the mounting mast influences the increase in maximum pressure on the model surface, which may alter the local aerodynamics of the aircraft. The greatest influence of the mast is observed at an angle of 0° , which may mean that in this configuration, the interaction of air streams with the mast is the strongest. And at an angle $\alpha = 20^{\circ}$, the mast itself does not generate high pressure, which may indicate other dominant aerodynamic effects in this configuration.

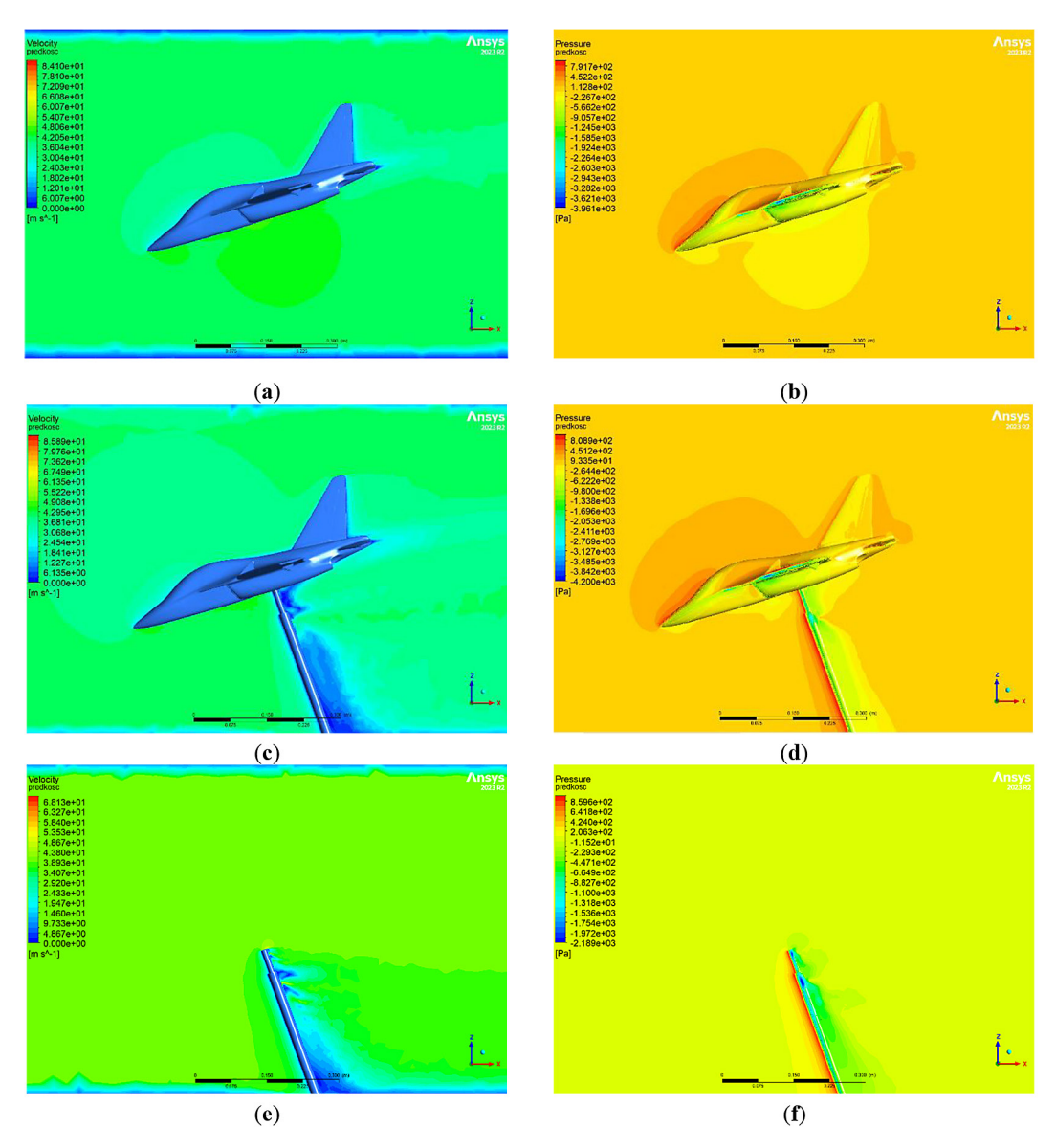


Figure 10. Comparison of velocity contours (left) and pressure contours (right) for an angle of attack $\alpha = -20^{\circ}$ for the considered geometry: (a), (b) variant I; (c), (d) variant II; (e), (f) variant III

Analysis of the lowest pressure values in the analyzed area indicates that variant II (aircraft + mast) exhibits greater negative pressures than variant I. Variant III (mast alone) exhibits significantly lower negative pressures than the aircraft itself, suggesting that its influence on pressure is different than in the case of the entire aircraft model. The largest difference between variants II and I occurs at an angle $\alpha = 20^{\circ}$ (-239 Pa), while for angles α = 0° and $\alpha = 20^{\circ}$, the differences are smaller. The mast in variant II causes a significant increase in negative pressure (-4200 Pa vs. -3961 Pa), which means that it disturbs the flow around the model and may lead to a change in lift on the aircraft model. The mast alone (variant III) has a significantly lower negative pressure (-2189 Pa), which

in turn suggests that it does not generate significant aerodynamic effects related to lift.

DISCUSSION

The analysis presented above aimed to understand the mutual aerodynamic interactions of the distinguished elements (aircraft and mast). By having the calculation results for the three analyzed variants, it is possible to perform an analysis of the mast's influence, which is used during wind tunnel testing. It should be emphasized that during tunnel tests, due to the use of an external balance, it is not possible to read the forces and moments acting only on the test object. The

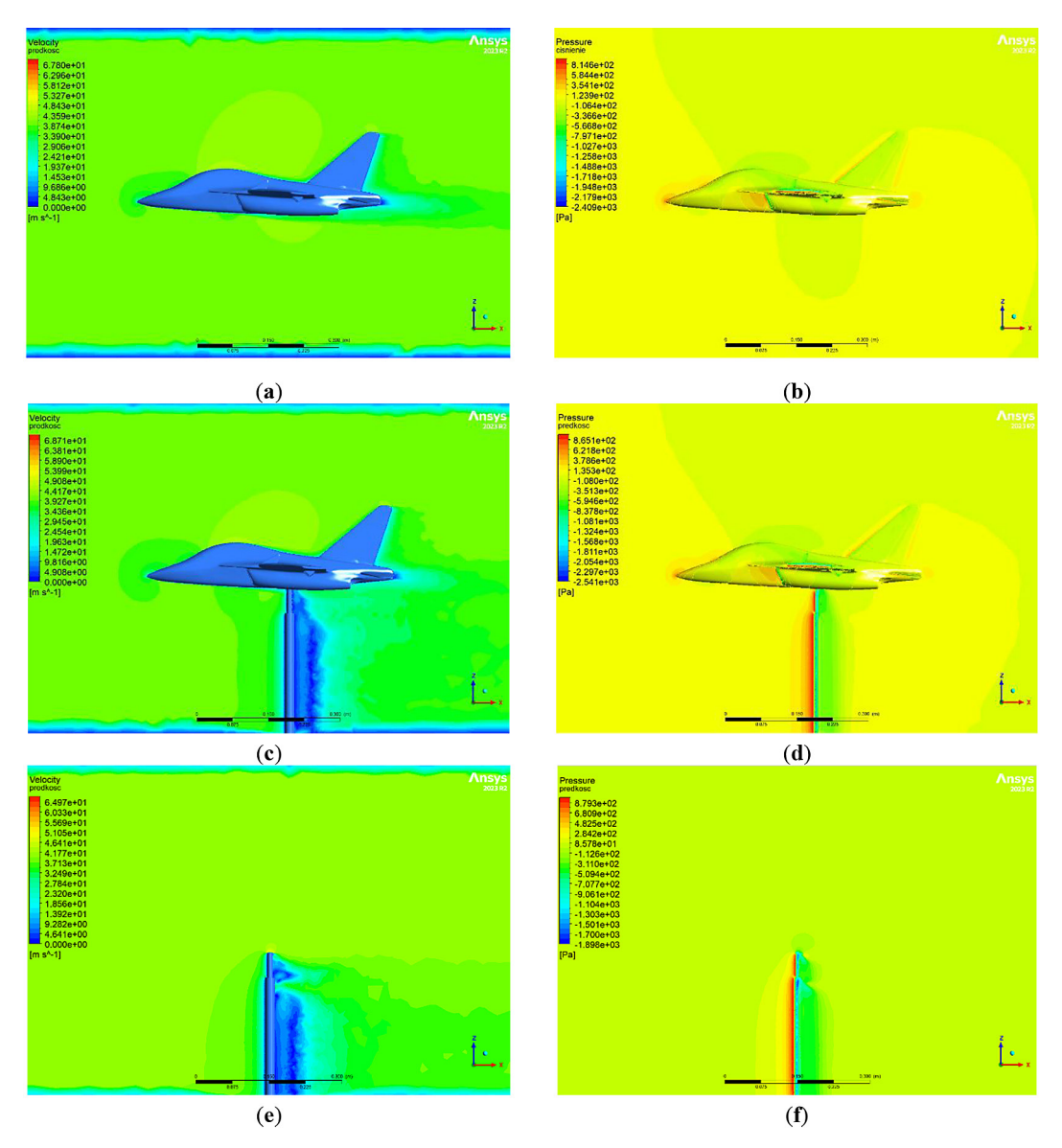


Figure 11. Comparison of velocity contours (left) and pressure contours (right) for an angle of attack $\alpha = 0^{\circ}$ for the considered geometry: (a), (b) variant I; (c), (d) variant II; (e), (f) variant III

reading of these quantities is done for the set: test object (e.g., aircraft) together with the mast.

Figures 13 and 14 compile the basic characteristics obtained by three different methods. The most important aspect is determining the influence of the mast on the obtained characteristics. First, the characteristic of the C_x coefficient was analyzed. The characteristics for methods (2) and (3) generally show a similar shape to the characteristic for method (1). However, there are some differences in the C_x coefficient values for individual angles of attack. The largest differences were observed for extreme angles of attack, especially for the angle -20° , where the C_x coefficient for methods (2) and (3) is greater than for method (1). In the case of the second method (2),

the minimum absolute difference compared to method (1) is only -0.00012, and the maximum is 0.02418. For method (3), this difference was 0.00067 and 0.01773, respectively.

In the case of the C_z coefficient for methods (2) and (3), a similar trend was obtained to the reference characteristic obtained by method (1). However, there are some differences in the C_z coefficient values for individual angles of attack. The largest differences appear for angles of attack -20° and 8° , where the C_z values for methods (2) and (3) are significantly different from the reference (method 1). Despite this, both methods showed agreement with the reference characteristic (1) at a high level, as in the case of the second method (2), the minimum absolute difference

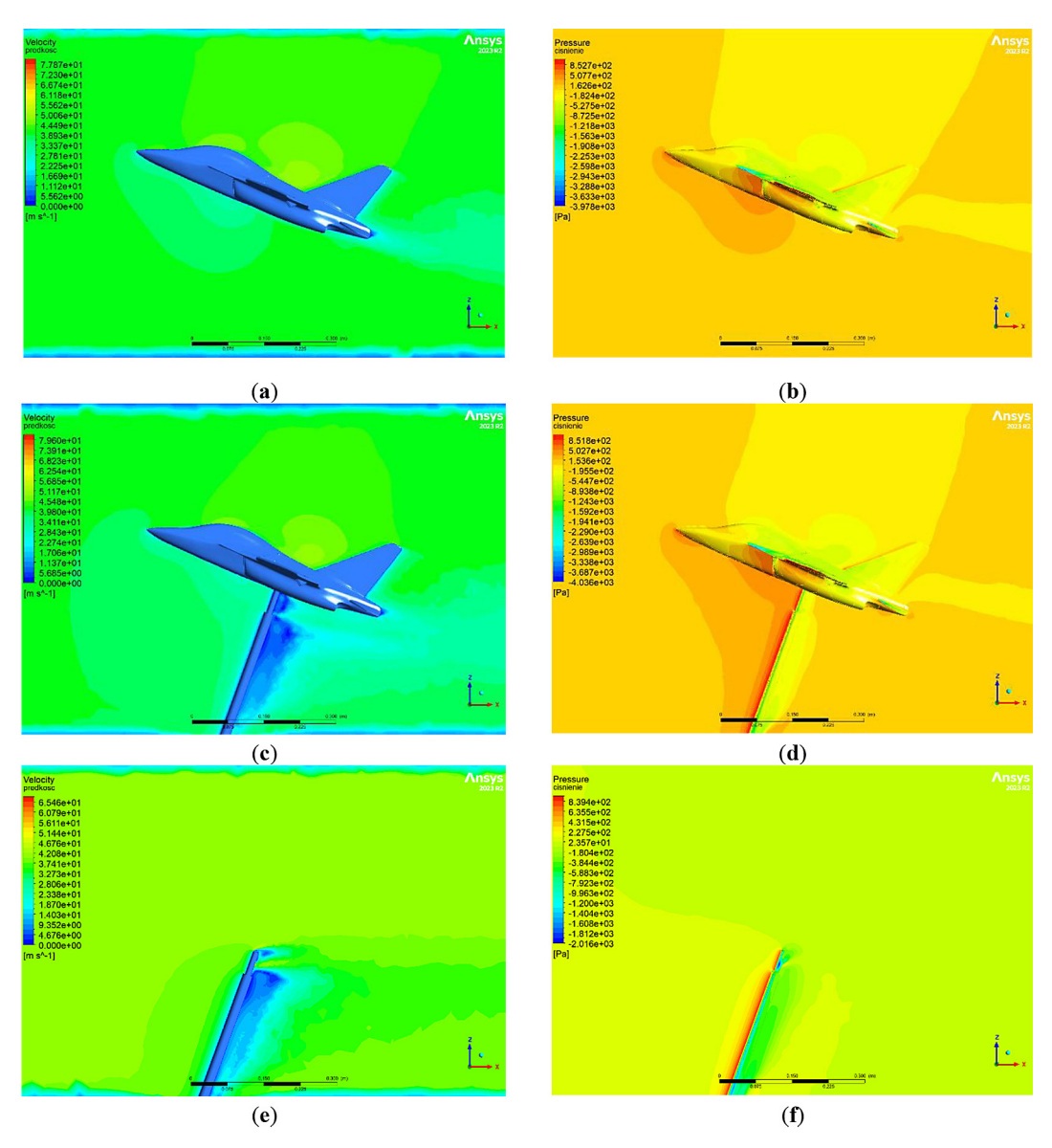


Figure 12. Comparison of velocity contours (left) and pressure contours (right) for an angle of attack $\alpha = 20^{\circ}$ for the considered geometry: (a), (b) variant I; (c), (d) variant II; (e), (f) variant III

compared to method (1) was only -0.00208, and the maximum was -0.05298. For method (3), it was -0.00187 and 0.05009, respectively.

Referring to the results presented in Figure 9, the mast is characterized by its own drag and lift coefficients. The study conducted by Haque et al. [18] in a low-speed wind tunnel showed that a diamond-shaped strut generates less lift compared to a cylindrical support. The obtained lift coefficient at a velocity of 40 m/s was approximately 0.002, while the drag coefficient was around 0.01. Mouton et al. [24] investigated the influence of a cylindrical support during tests of an aircraft model. Experimental results revealed that the drag coefficient depended on the angle of attack and exhibited significant scatter. The drag coefficient varied

between approximately -0.0035 and 0.0055. The effect of the support on axial force was well predicted by simulations and fell within the experimental uncertainty range for all tested angles of attack. The lift coefficient ranged from about 0.0055 to 0.0160. The coefficient values obtained by the authors of this study for the tested strut are 0.0041 for the lift coefficient and 0.0725 for the drag coefficient at zero angle of attack.

The situation is different with the pitching moment coefficients C_{My} . Both methods (2) and (3) give results that differ from method (1). These differences vary depending on the angle of attack. However, it should be noted that methods (2) and (3) give results that are close to each other (especially in the area of positive angles of attack), but

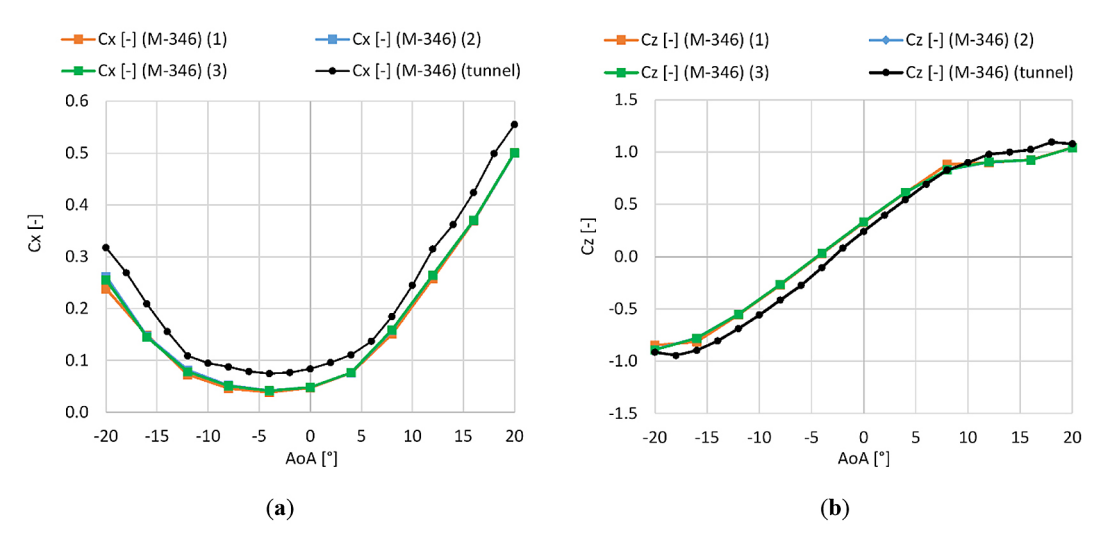


Figure 13. (a) Relationship of drag coefficient and (b) lift coefficient to angle of attack

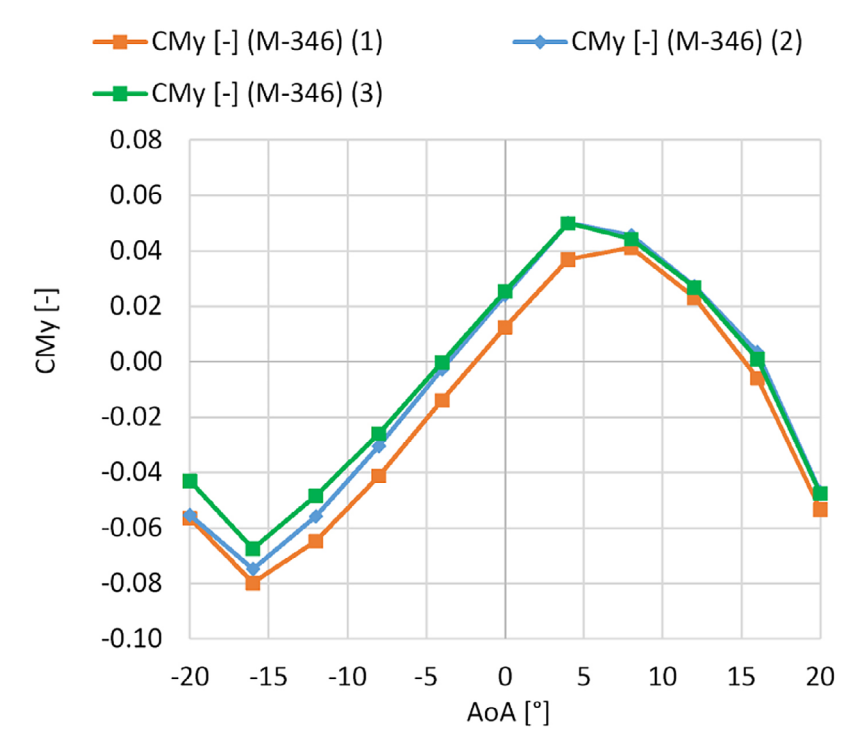


Figure 14. Relationship of pitching moment coefficient to angle of attack

differ from method (1). The maximum coefficient difference for method (2) compared to method (1), which is 0.01320, occurred at an angle of 4° , and the maximum coefficient difference for method (3) compared to (1), which is 0.01635, occurred at an angle of -12° . In summary, both methods (2) and (3) show clear differences compared to the reference (method 1).

In addition to the comparative analysis of three different methods for obtaining aerodynamic characteristics numerically, it is worth referring to the results from the wind tunnel experiment, some of which were included in [43]. To this end, the results obtained from wind tunnel tests were also included in Figure 13. Based on the presented data, a comparative analysis of numerical and experimental results can be performed. In the case of the drag coefficient, all three computational methods show very similar values and behave consistently with the experimental results. The largest errors occur in the range of angles from -8° to 0° , which results from the fact that the C_x values in this range are low, so even a small difference causes a high percentage error. For

larger angles of attack, there is relatively good agreement, and for example, for $\alpha \ge 8^{\circ}$, the relative error drops below 20%, and for $\alpha = 20^{\circ}$, it reaches the lowest value of approximately 9.8%. This means that the models accurately represent drag for larger angles of attack. Thus, although the relative error is large for small C_{x} values, the overall trend of the results is correct. In the case of the lift coefficient, good agreement also occurs for large angles of attack. For $\alpha \ge 8^{\circ}$, the relative error does not exceed 10%, which means that the models accurately represent lift in this range. The problematic range of low angles, where the relative errors are much larger, also results from the fact that in this range the force values are low, so even a small difference causes a high percentage error. Very good convergence of method 2 occurs for $\alpha = 8^{\circ}$, where almost identical results were obtained as in the wind tunnel (relative error of only 0.2%). Numerical model can be used for aerodynamic analysis, but in the future, they can be calibrated to obtain even smaller relative errors.

CONCLUSIONS

The conducted analysis allowed for a detailed evaluation of the aerodynamic interactions of the support structure on the aircraft model in the measurement chamber of a closed-circuit wind tunnel. Based on the conducted calculations, the following conclusions were drawn. The model support consisted of a cylindrical mast. At one of its ends, the tested model was installed, and at the other, an external force balance was located. Tests and numerical calculations confirm the significant contribution of the mast to the total drag force. For instance, at $\alpha = -20^{\circ}$, the mast contributed approximately 24% of the total drag coefficient. The support system of a research object, such as the light combat aircraft M-346 Master, cannot be ignored in the analysis of its characteristics. A very good convergence of the $C_{\rm c}(\alpha)$ and $C_{\rm c}(\alpha)$ characteristics of the test object itself, obtained by subtracting the support, was confirmed. In the range of $\alpha = 8^{\circ}$ to 20° , the relative error in lift coefficient remained below 10%, and for $\alpha = 8^{\circ}$, it was as low as 0.2%. Additionally, low support interference on the $C_{\epsilon}(\alpha)$ and $C(\alpha)$ characteristics of the aircraft model was achieved.

Although the mast introduces some disturbances in the total lift coefficient C_z , it does not

have a decisive influence on the aerodynamic characteristics of the entire system. Its influence is noticeable but relatively small. For example, at $\alpha=20^\circ$, the total lift coefficient decreased from 1.042 (aircraft only) to 1.020 (aircraft + mast), indicating a change of approximately 2.1%. This means that the experimental results obtained from wind tunnel tests of the aircraft can be considered close to the actual results without considering the mast. However, this aspect should be taken into account in precise analyses.

In the case of small angles of attack, particularly from $\alpha = -4^{\circ}$ to $\alpha = 4^{\circ}$, special attention should be paid to subtracting the drag from the mast to obtain accurate results for the aerodynamic characteristics of the aircraft itself.

The analysis of three methods for assessing the influence of the mast allowed for drawing conclusions related to eliminating the influence of this object on the aerodynamics of the tested model. In the case of the C_x coefficient, both methods (2) and (3) show small deviations from the reference characteristic (obtained using method 1). The largest differences occurred for extreme angles of attack, especially for an angle of attack of -20°. For method (2), the maximum difference compared to method (1) was 0.02418, while for method (3), it was 0.01773. In general, method (2) is closer to the reference (method 1) compared to method (3). However, both variants are acceptable in the context of agreement with the reference characteristic. The situation is similar in the case of the C_z coefficient. For method (2), the maximum difference was -0.05298, while for method (3), it was 0.05009.

The developed aerodynamic characteristics can be used to develop an algorithm for correcting wind tunnel test results to improve the quality of modeling the real object under experimental conditions. To verify the presented results regarding the impact of the support, further research involving additional objects is planned.

Acknowledgements

This work was prepared in part during an international scientific internship undertaken by Zbigniew Czyż from Polish Air Force University (Poland) at the Institute of Mechanical Science of Vilnius Gediminas Technical University. The internship took place from August 16 to September 16, 2024.

REFERENCES

- Ciliberti D., Buonagura G., Nicolosi F. Longitudinal wind tunnel tests of the PROSIB 19-pax airplane. Appl. Sci. 2023;13:11928. https://doi.org/10.3390/ app132111928
- Czyż Z., Wendeker M. Measurements of aerodynamic interference of a hybrid aircraft with multirotor propulsion. Sensors 2020;20(12):3360. https://doi.org/10.3390/s20123360
- 3. Szwedziak K., Łusiak T., Bąbel R., Winiarski P., Podsędek S., Doležal P., et al. Wind tunnel experiments on an aircraft model fabricated using a 3D printing technique. J. Manuf. Mater. Process. 2022;6(1):12. https://doi.org/10.3390/jmmp6010012
- Britt R., Ortega D., Tigue J.M., Scott M. Wind tunnel test of a very flexible aircraft wing. In: Proceedings of the 53rd AIAA/ASME/ASCE/AHS/ ASC Structures, Structural Dynamics and Materials Conference. Honolulu, HI, USA: AIAA; 2012. p. 1464. https://doi.org/10.2514/6.2012-1464
- Czyż Z., Karpiński P., Skiba K. Wind tunnel investigation of the propellers for unmanned aerial vehicle.
 In: Proceedings of the 2021 IEEE 8th International Workshop on Metrology for AeroSpace (MetroAeroSpace). IEEE; 2021. p. 672–6. https://doi.org/10.1109/MetroAeroSpace51421.2021.9511724
- Czyż Z., Karpiński P., Skiba K., Wendeker M. Wind tunnel performance tests of the propellers with different pitch for the electric propulsion system. Sensors 2021;22(1):2. https://doi.org/10.3390/ s22010002
- Skrucany T., Sarkan B., Gnap J. Influence of aerodynamic trailer devices on drag reduction measured in a wind tunnel. Eksploat. Niezawodn. 2016;18(1):151–4. https://doi.org/10.17531/ ein.2016.1.20
- 8. Ivánková O., Hubová O., Macák M., Vojteková E., Konečná L.B. Wind pressure distribution on the façade of stand-alone atypically shaped highrise building determined by CFD simulation and wind tunnel tests. Designs 2022;6(5):77. https://doi.org/10.3390/designs6050077
- Gierz Ł. The method and a stand for measuring aerodynamic forces in every plane on the basis of an image analysis. Proc. SPIE 2019;11179:111793F. https://doi.org/10.1117/12.2539963
- Bansmer S.E., Baumert A., Sattler S., Knop I., Leroy D., Schwarzenboeck A., et al. Design, construction and commissioning of the Braunschweig Icing Wind Tunnel. Atmos. Meas. Tech. 2018;11(6):3221–49. https://doi.org/10.5194/amt-11-3221-2018
- 11. Plaza del Pino J.C., Terroba Ramírez F., García-Magariño A., Atienza Pascual R., Mora Nogués J. Practical design of a low-cost icing wind tunnel for unmanned aerial vehicle testing in a limited

- space. Appl. Sci. 2024;14(16):6928. https://doi.org/10.3390/app14166928
- 12. Ćurčić D., Samardžić M., Marinkovski D., Rajić Z., Anastasijević Z. Model sting support with hard metal core for measurement in the blowdown pressurized wind tunnel. Measurement 2016;79:130–6. https://doi.org/10.1016/j.measurement.2015.11.002
- 13. Ghika S.A., Penela Guerrero L.A. Mechanical design, analysis, and manufacturing of wind tunnel model and support structure [master's thesis]. Stockholm, Sweden: KTH Royal Institute of Technology; 2021.
- 14. Della Corte B., Perpignan A.A., van Sluis M., Rao A.G. Experimental and computational analysis of model–support interference in low-speed wind-tunnel testing of fuselage-boundary-layer ingestion. MATEC Web Conf. 2019;304:02020. https://doi.org/10.1051/matecconf/201930402020
- 15. Ericsson L.E., Reding J.P. Review of support interference in dynamic tests. AIAA J. 1983;21(12):1652–66. https://doi.org/10.2514/3.60166
- Tuttle M.H., Gloss B.B. Support interference of wind tunnel models: a selective annotated bibliography. Washington (DC): NASA; 1981. NASA Technical Memorandum 81909.
- 17. Carter E.C. Interference effects of model support systems. Neuilly-sur-Seine, France: AGARD; 1973. AGARD Report No. 601.
- 18. Haque A.U., Asrar W., Omar A.A., Sulaeman E. Effect of diamond shaped strut with cylindrical pitch rod in subsonic wind tunnel testing. Measurement 2017;99:1–6. https://doi.org/10.1016/j.measurement.2016.12.016
- 19. Biermann D., Herrnstein W.H. Jr. The interference between struts in various combinations. Washington (DC): National Advisory Committee for Aeronautics; 1934. NACA Report No. 468.
- 20. Rist M. Computational investigation of wind tunnel support interference. In: Proceedings of the 25th Plasmadynamics and Lasers Conference. AIAA; 1994; 2602. https://doi.org/10.2514/6.1994-2602
- 21. Czyż Z., Karpiński P. Numerical analysis of the impact of sideslip angle on load of the gyrocopter stabilizers. Aviation 2019;23(3):114–22. https://doi.org/10.3846/aviation.2019.11924
- 22. Semkło Ł., Gierz Ł. Analysis of flow through channel with mounted blades. MATEC Web Conf. 2018;240:03012. https://doi.org/10.1051/matecconf/201824003012
- 23. Semkło Ł., Gierz Ł. Numerical and experimental analysis of a centrifugal pump with different rotor geometries. Appl. Comput. Sci. 2022;18(4):82–95. https://doi.org/10.35784/acs-2022-30
- 24. Mouton S. Numerical investigations of model support interference in subsonic and transonic wind

- tunnels. In: Proceedings of the ODAS 2007 8th ONERA-DLR Aerospace Symposium. ONERA-DLR; 2007.
- Sieradzki A., Kwiatkowski T., Krysztofiak G., Ruchała P., Łukasik B., Turner M. Analysis of the turbulence field in a low-speed fan test rig with distorted inflow. Adv. Sci. Technol. Res. J. 2025;19(4):386– 400. https://doi.org/10.12913/22998624/200867
- Pędzisz I., Magryta P., Pietrykowski K. Computational fluid dynamics studies of a vertical axis wind turbine with a variable swept area. Adv. Sci. Technol. Res. J. 2024;18(2):333–48. https://doi.org/10.12913/22998624/185255
- 27. Li S., Liu D., Li Q. The optimal design of a wind tunnel model sting system based on the CFD method. Int. J. Heat Technol. 2015;33(4):137–44. https://doi.org/10.18280/ijht.330417
- 28. Wubben F., Maseland H. Verification of wind tunnel model support and wall interference assessments in DNW-HST by CFD simulations. Neuilly-sur-Seine, France: NATO Science and Technology Organization; 2018. Report No. STO-MP-AVT-284-5.
- Fischer O., Kuthada T., Widdecke N., Wiedemann J. CFD investigations of wind tunnel interference effects. SAE Tech. Pap. 2007;2007-01-1045. https:// doi.org/10.4271/2007-01-1045
- 30. Waldmann A., Lutz T., Krämer E. Wind tunnel support system influence on NASA common research model at low-speed conditions. J. Aircr. 2018;55(5):1762–72. https://doi.org/10.2514/1. C034440
- 31. Rogowski K., Mikkelsen R.F., Michna J., Wiśniewski J. Aerodynamic performance analysis of NACA 0018 airfoil at low Reynolds numbers in a low-turbulence wind tunnel. Adv. Sci. Technol. Res. J. 2025;19(2):136–50. https://doi.org/10.12913/22998624/195556
- 32. Ocokoljić G., Rašuo B., Kozić M. Supporting system interference on aerodynamic characteristics of an aircraft model in a low-speed wind tunnel. Aerosp. Sci. Technol. 2017;64:133–46. https://doi.org/10.1016/j.ast.2017.01.021
- 33. Hetherington B., Sims-Williams D.B. Wind tunnel model support strut interference. SAE Tech. Pap. 2004;2004-01-0806. https://doi.org/10.4271/2004-01-0806
- 34. Hetherington B., Sims-Williams D.B. Support strut interference effects on passenger and racing car wind tunnel models. SAE Tech. Pap. 2006;2006-01-0565. https://doi.org/10.4271/2006-01-0565

- 35. Kohzai M., Sudani N., Yamamoto K., Ueno M., Hashimoto A. Experimental and numerical studies of support interference in the JAXA 2m × 2m transonic wind tunnel. In: Proceedings of the 27th AIAA Aerodynamic Measurement Technology and Ground Testing Conference. AIAA; 2010; 4200. https://doi.org/10.2514/6.2010-4200
- 36. Kohzai M., Ueno M., Koga S., Sudani N. Wall and support interference corrections of NASA common research model wind tunnel tests in JAXA. In: Proceedings of the 51st AIAA Aerospace Sciences Meeting Including the New Horizons Forum and Aerospace Exposition. AIAA; 2013; 963. https:// doi.org/10.2514/6.2013-963
- 37. Russo S., Mueller J., Paletta N., Adden S., Ruiz-Calavera L.P. Numerical prediction of the strut interference on a regional aircraft wind-tunnel model. In: Proceedings of the 6th European Conference on Computational Mechanics (ECCM 6) and 7th European Conference on Computational Fluid Dynamics (ECFD 7); 2018.
- 38. Lee S., Song H., Park G. Study of strut interference in high-speed flows. Exp. Fluids 2020;61(5):105. https://doi.org/10.1007/s00348-020-2934-8
- Russo S., Müller J., Alderman J., Paletta N., Adden S., Ruiz-Calavera L.P. A CFD study on the strut interference on a regional aircraft wind-tunnel model. IOP Conf. Ser. Mater. Sci. Eng. 2021;1024(1):012047. https://doi.org/10.1088/1757-899X/1024/1/012047
- 40. Hebbar S., Sommers J. Wind tunnel studies of support strut interference on a 3 percent YF-17 fighter aircraft model at high angles of attack. In: Proceedings of the Flight Simulation Technologies Conference and Exhibit. AIAA; 1990; 3083. https://doi.org/10.2514/6.1990-3083
- 41. Beyers M.E. Unsteady wind-tunnel interference in aircraft dynamic experiments. J. Aircr. 1992;29(6):1122–9. https://doi.org/10.2514/3.46294
- 42. Placek R., Ruchała P., Stryczniewicz W. Ground effect influence on the aerodynamic characteristics of ultralight high-wing aircraft wind tunnel tests. J. KONES 2017;24(1):183–90. https://doi.org/10.5604/01.3001.0010.2931
- 43. Czyż Z., Karpiński P., Ruchała P., Zahorski T. Preliminary measurements for the identification of the influence of the test object support on the aerodynamic characteristics. In: Proceedings of the 2024 11th International Workshop on Metrology for AeroSpace (MetroAeroSpace). IEEE; 2024; 399–404. https://doi.org/10.1109/MetroAeroSpace61015.2024.10591576